A NEW PARAMETERIZATION OF AN EMPIRICAL MODEL FOR WIND/OCEAN SCATTEROMETRY

Peter M. Woiceshyn
Jet Propulsion Laboratory, California Institute of Technology,
Pasadena, CA, USA
Morton G. Wurtele
Department of Atmospheric Sciences, UCLA, Los Angeles, CA, USA
Dale H. Boggs
dB Systems, Ltd., La Canada-Flintridge, CA, USA
Lawrence F. McGoldrick
Applied Physics Laboratory, Johns Hopkins University, Laurel, MD, USA
Steven Peteherych
Atmospheric Environment Service, Downsview, Ont., Canada

1.   ABSTRACT

This study reveals that the power-law form of the Seasat A Scatterometer System (SASS) empirical backscatter-to-wind model function does not uniformly meet the instrument performance specification requirements; viz., error in derived wind speed < max $(2 \text{ ms}^{-1}, 10$ percent), over the range 4 to 24 ms^{-1}. Analysis indicates that the horizontal-polarization (H-Pol) and vertical-polarization (V-Pol) components of the benchmark SASS1 model function (Schroeder, et al 1982b) yield self-consistent results only for a small mid-range of speeds at larger incidence angles, and for a somewhat larger range of speeds at smaller incidence angles. The present approach differs from previous calibration studies (e.g., Jones et al., 1982): here the model's internal V-Pol vs. H-Pol consistency is examined by the use of a set of pair-wise collocated SASS-produced winds, where one member of a wind pair derives from only V-Pol backscatter measurements and the other from only H-Pol measurements. This data set was created by extracting all pairs of SASS GDR (Boggs, 1982) winds of the form (U_{VV}, U_{HH}) such that U_{VV} and U_{HH} are contemporaneous and are separated by no more than 50 km, and contains 377,289 such pairs.

Comparison of SASS1 to _in situ_ data over the Gulf of Alaska region further underscores the shortcomings of the power-law form. We find that the slope of the V-Pol-backscatter-measurement vs. wind-speed relationship for speeds greater than 10 ms^{-1} is less than that given by SASS1. Taken together, this _in situ_ comparison and the SASS1 V-H self-consistency study indicate that H-Pol-backscatter vs. wind-speed slope is greater than V-Pol-backscatter slope for speeds above 10 ms^{-1}, with the reverse holding for speeds under 10 ms^{-1}. Thus H-Pol backscatter shows greater sensitivity to wind speed variation at higher winds, and less at lower winds, than does V-Pol backscatter.

Finally, a physically-based empirical SASS model is proposed which corrects some of the deficiencies of power-law models like SASS1. The new model allows the mutual determination of sea surface wind stress and wind speed in a consistent manner from SASS backscatter measurements. In contrast, the SASS1 model only determines the wind speed.

57

INTRODUCTION:

The oceans cover 70 percent of the Earth's surface, and the paucity of weather observations over these huge areas has always been a great handicap to wind and wave forecasting. This condition was alleviated for the short three summer months in 1978 when NASA flew the Seasat satellite, which carried three wind measuring instruments Hicps and Wilson, 1983); only one of which we are concerned with here.

The Seasat A Scatterometer System (SASS) was a 14.6 GHz (2.1 cm) active microwave radar designed to permit inference of the ocean surface wind from precise measurements of the backscatter of emitted radiation by gravity-capillary waves on the sea surface. The received return, expressed as the normalized radar cross section (NRCS or σ°), from the four dual-polarized, x-oriented antennae may be directly related to the surface wind speed through a geophysical "model function", constructed by means of a combination of theory and experiment (Schroeder et al., 1982b). The wind direction, however, is not uniquely determined (Wurtele et al., 1982; Peteherych et al., these Proceedings). This paper will not be concerned with the multiple wind-direction ambiguity (i.e., the "alias") problem.

The fundamental validations of SASS are contained in the articles by Jones et al. (1982), Schroeder et al (1982a and 1982b), Wurtele et al. (1982), Brown (1983), reporting on the large cooperative Gulf of Alaska Seasat Experiment (GOASEX) and Joint Air-Sea Interaction Experiment (JASIN) workshops, out of which came the benchmark SASS1 "model function". The SASS1 relates the NRCS to the wind field parameters, speed and direction, relative to: the incidence angle (Θ) of the radar radiation arriving at the sea surface, the azimuth angle (χ) of the wind direction relative to the radar beam illumination at the surface, and the polarization type (ϵ) of the incident radar radiation; i.e., vertical polarization (V-POL or V-POLE) or horizontal polarization (H-POL or H-POLE). A review of the history of the relationship between NRCS and wind speed at microwave frequencies is given by Moore and Fung (1979), Boggs (1981), and Schroeder et al (1982b). The basic assumptions are that the relationship between the NRCS and the wind speed is a power law (described below), and that there is no dependence on sea surface parameters such as temperature, viscosity, and surface tension. The constants of the power law were evaluated by "tuning" the model to a "surface truth" comparison wind data set in JASIN, where the sea surface temperature was constant (about 12°C) and the wind speed range was small (4 - 16 ms^{-1}, Boggs, (1981)). The Seasat specifications for the SASS were: wind speed measurement range of 4 to 24 ms^{-1} with an accuracy of $\pm$ 2 ms^{-1} or 10%, whichever is greater; and wind direction of 0 to 360 to within 20 degrees (Jones et al., 1982). Jones et al. claim that the SASS model function, SASS1 (Schroeder at al, 1982b) yield accuracies better than the Seasat specifications over the 0 to 16 ms^{-1} range of winds observed during JASIN. This paper outlines problems with the above assumptions in the SASS model function, particularly at larger wind speeds and incidence angles. The results here will begin to show that SASS did not uniformly meet its performance specifications over the

58

wind speed range placed by the Seasat Project, and that a certain fraction of the 16 million SASS observations may be in error by more than the performance specifications allowed. In spite of this, the study by Peteherych et al. (1984, these Proceedings) clearly shows that the scatterometer system "works" in defining and locating the weather patterns. Therefore, the SASS data record derived using SASS1 is eminently qualified for many meteorological and oceanographic purposes.

The presentation of our results to date is organized into three parts:

(1)   The first part is a restriction to aspects of the SASS1 model function that can be treated without reference to surface truth. Here we use various checks in order to test the internal consistency of the model function, both quantitatively and in its form. The data set used for this study consists of 377,289 pairs of SASS wind speeds of the form (U_{VV}, U_{HH}), where each member of the pair is derived separately from V-Pol and H-Pol NRCS's such that U_{VV} and U_{HH} are located within 50 km of each other. This data set is an extraction of all such pairs of SASS/SASS1 derived wind speeds from the complete Seasat mission data set resident on the Pilot Ocean Data System (PODS) at JPL.

(2)   The second study makes some comparisons of wind speeds from in situ wind fields derived from ships and buoy reports, to SASS1 and other scatterometer model functions.

(3)   A new model is then hypothesized to reduce or eliminate some of the discrepancies shown by the studies cited above. This model differs in form from previous models, including SASS1, but should be considered as a modification of these, rather than as a construction from first principles.

3.   INTERNAL CONSISTENCY CHECK OF THE SASS1 MODEL

The SASS operated in any one of 8 modes of antenna/polarization combinations during which a four antenna-beam/polarization sequence was cycled through. The principal operational mode was mode 1. This resulted in sequencing the four antennas through vertical polarization on both sides of the spacecraft. The present study, however, is based exclusively on data taken during modes 3 and 4. These two modes generated vertical and horizontal polarization sequencing on the left side of the spacecraft only (mode 3) or on the right side only (mode 4). This resulted in the determination of SASS winds derived from either V-Pol NRCS data or H-Pol NRCS data in nearby locations.

Figure 1 illustrates samples of SASS wind fields in the form of direction ambiguity "aliases" (the X's with noted speeds in meters per

second) derived with the SASS1 model function. The wind solutions in
the left panel are computed from V-Pol-only data, and in the right
panel from H-Pol-only data. These measurements were taken during a
single SASS pass on the morning of September 17, 1978 in the vicinity
of the HMS Ark Royal aircraft carrier (marked A) and the NATO fleet
operating in the southern Norwegian Sea (Fett and Bohan (1981)).   The
flag symbol at A notes that the Ark Royal reported winds of 55 knots
(about 28 meters per second) in magnitude by the anemometer mounted 18
meters above the ocean surface.   Besides the near agreement   between
Ark Royal and the H-Pol winds (U_{HH}, at 19.5 m elevation), note the
large disagreement   between   the V-Pol winds (U_{VV} , at 19.5 m
elevation) and U_{HH} .   We also discovered similar disagreements
between U_{VV} and U_{HH} for the high winds in the SASS passes over the
storm which damaged the Queen Elizabeth II luxury liner on September
11, 1978.
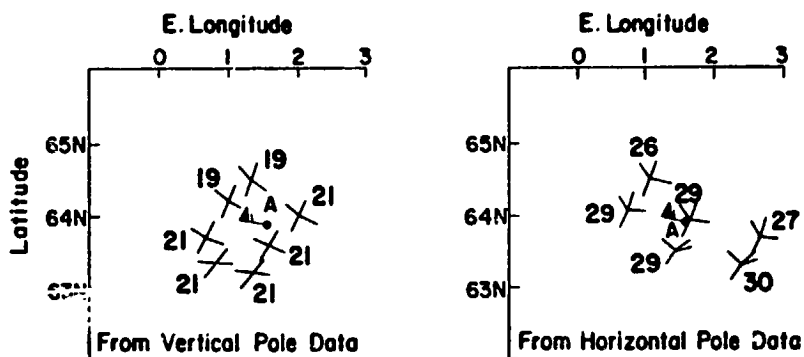
Having concluded from these specific examples that serious
polarization inconsistencies exist in SASS1, we turn to a more
systematic and fundamental approach.   We first note that the SASS1
model function relates the NRCS intensity to the surface marine wind
field by a power law:

$$NRCS = g\ (\theta, \chi, \epsilon)\ U^{H(\theta, \chi, \epsilon)} \tag{1}$$

Since the NRCS is usually expressed in decibel (dB) units,
Equation (1) is written in its logarithmic form:

$$\sigma^{\circ} = NRCS\,(dB) = 10\left\{ G(\theta, \chi, \epsilon) + H(\theta, \chi, \epsilon)\ \log_{10} U \right\} \tag{2}$$

where $G = \log_{10} g$. The parameters θ, χ, and ϵ are defined above. It
is important to observe that this power-law relationship is an
established conventional formulation which seems to have arisen (e.g.,

Valenzuela et al, 1971) as a convenient curve-fitting technique, without any particular physical rationale. The official SASS1 model function is in the form of tables of G and H functions for two-degree intervals of incidence angle (Θ) and ten-degree intervals of azimuth angle (χ) for both V-Pol and H-Pol NRCS (Schroeder et al. 1982b, table 2). As remarked above, these table values were tuned to the high-quality JASIN surface wind fields data set. The total data set was derived from about 700 wind measurements with an upper bound of 16 ms^{-1}, 66 of which are in the low-speed interval 0 to 6 ms^{-1}. Insofar as wind speed is concerned, it is fair to say that SASS1 was tuned to a very limited data set.

If we take Θ = 38 degrees and χ = 0 degrees as typical values, we find in Schroeder et al. (1982b) the table entries for SASS1:

			G	H
ϵ	=	V-Pol:	-2.953	1.690
ϵ	=	H-Pol:	-3.368	1.823
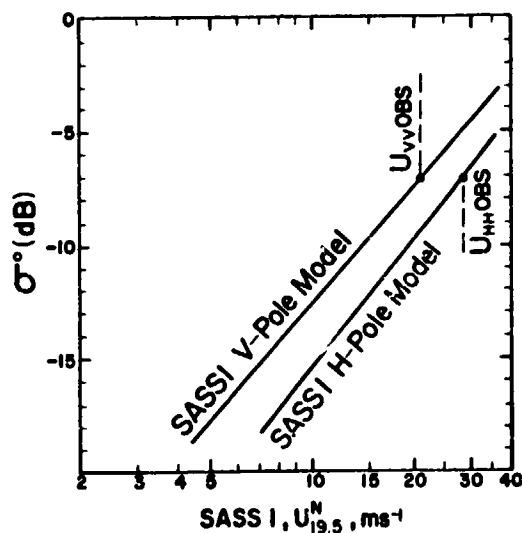
Figure 2. A graphical depiction of SASS1 power-law function, Eq.(2), for the conditions Θ = 38, χ = 0, for both V-Pol and H-Pol NRCS (σ^o). Shown also are representative values from Fig. 1. The superscript N on U (the windspeed) denotes winds corrected to neutral stratification condions for the atmospheric surface layer. The subscript 19.5 on U indicates the reference height for U above sea level. Both subscripts and superscripts have been dropped elsewhere in the figures and text.

Thus, on a σ^o vs log U diagram the H-Pol plot will be below the V-Pol plot, with a slightly greater slope, as seen in Figure 2. Referring to Figure 1, we may take the mean H-Pol wind speed as 29 ms^{-1} and the V-Pol as 21 ms^{-1}. If these two speeds are mapped into NRCS values via the SASS1 table entries -- indicated by the points U_{VV}OBS and U_{HH}OBS in Figure 2 -- we see that the resulting H-pol and V-pol NRCS's are approximately equal (~-7dB). These results at high winds have been anticipated. Valenzuela (1968) reported that "for very rough seas the cross-sections for horizontal polarization become comparable to, or greater, by a few decibels, than those for vertical polarizations; while for calm and moderate sea conditions, the cross sections for vertical polarization are always greater".

The discrepancy noted in the Ark Royal case is characteristic of the higher wind-speed range, as can be seen from the statistical presentation of Figure 3. Here the set of pair-

H-PUL VERSUS CO-LOCATED V-PCL WIND SPEED COMPARISON
ALL NON-NADIR INCIDENCE ANGLES
R.M.S SPEED BINS

48/48 POINTS

V-POL BIN-AVERAGED WIND SPEED, m/s
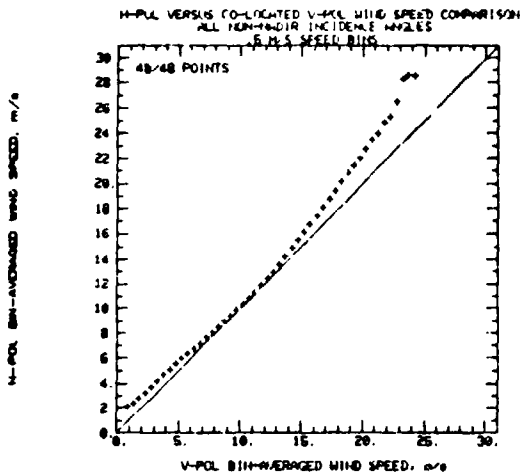
Figure 3. Statistical comparison of winds derived from the SASS1 V-Pol and H-Pol power law. 377,289 pairs of V-Pol and H-Pol wind data were sorted in one-half meter per second V-Pol wind bins.

V AND H POLARIZATIONS

+ V-Pole
✗ H-Pole

INCIDENCE ANGLE, DEG.
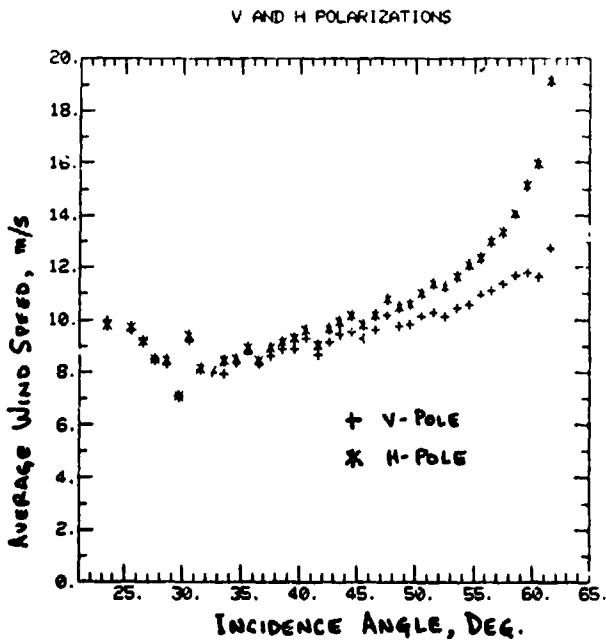
Figure 4. Consistency between winds derived from the SASS1 V-Pol and H-pol power law, Eq.(2), as a function of incidence angle. 377,289 pairs of V-Pol and H-Pol wind data were sorted in one degree incidence angle bands.

wise concurrent SASS V and H pol winds described above is examined in a V vs. H sense. The 377,289 V/H pairs were first sorted by V value into forty-eight 0.5 ms V-pol wind speed bands along the abscissa. Each ordinate point shown is then the mean speed of all the H values falling within a particular band. Note that this comparison does not depend on the quality of in situ data (except for the model-tuning JASIN data itself), but constitutes an internal consistency check on the SASS1 model function.

Figure 4 examines the incidence angle. This study shows differences and sensitivities of the mean wind speeds (grouped in one-degree incidence angle "bands") as a function of incidence angle. The trend in difference between V-Pol and H-Pol winds as a function of Θ, and the general dip of both VV and HH mean wind speeds as a function of Θ beg explanation. If the SASS1 were correcty specified, we would then expect constant and identical mean wind speeds as a function of Θ .

An examination of the sensitivity of SASS1 to wind speed, polarization, and incidence angle, is better displayed in Figure 5, which shows the bivariate frequency distribution of U_{VV} and U_{HH} in three-dimensional form as a function of incidence angle (noted to the right of each of the three distribution plots).
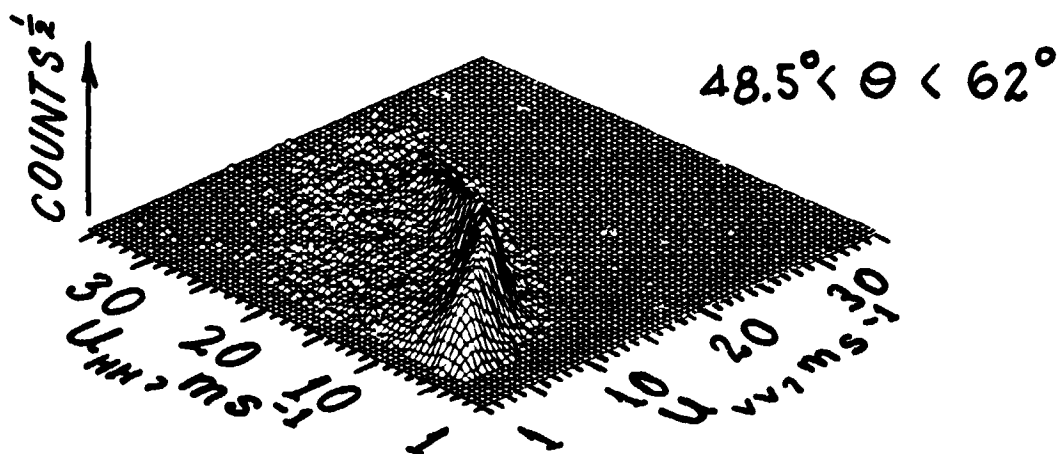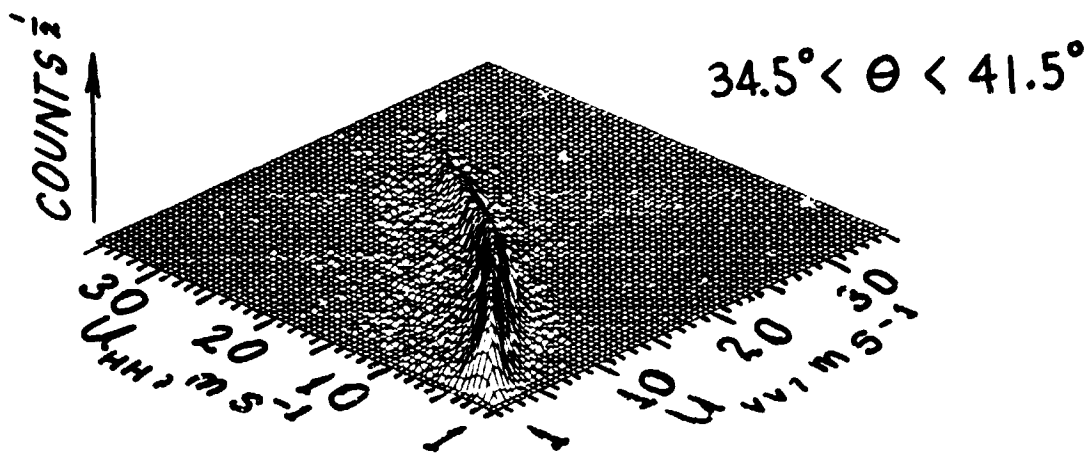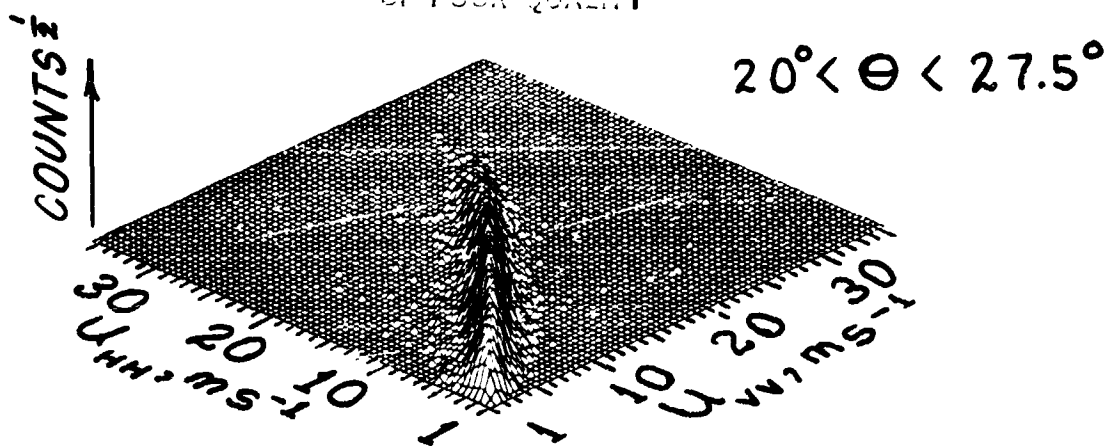
Figure 5. A 3-dimensional display of the characteristics of the bivariate frequency distribution (vertical scale) of collocated (within 50 KM) U_{VV}(right horizontal scale) and U_{HH}(left horizontal scale) derived from SASS1 for 3 different incidence angle (Θ) bands. The vertical scale is to the one-half power for ease of display of the characteristics. The wind data are sorted in one-half by one-half meter per second windspeed bins.

The paired U_{VV} and U_{HH} data set was sub-divided into one-half meter per second wind speed bins in U_{VV} and U_{HH}. These bins were further segregated into 5 incidence angle bands of about 75,000 pairs of measurements in each band. This incidence angle band breakdown is sufficient to indicate the trend of the data. The vertical scale is the square root of the number of pairs (counts) in each one-half by one-half meter per second bin to make the lower frequency counts visible and to ease analysis of the characteristics. The range of wind speeds shown is from one to 35 ms^{-1} for both U_{VV} and U_{HH}; the grid is one-half ms^{-1}. The data shows the best agreement between U_{VV} and U_{HH} for the lowest range of incidence angles (top panel), except at small winds where U_{HH} is greater than U_{VV} (data lying along the vertical diagonal would indicate exact agreement). The poorest agreement between U_{HH} and U_{VV} evidently is at the largest range of incidence angles. Here, U_{HH} is greater in magnitude for both the lowest and highest winds. In a small interval of midrange wind speeds, the agreement appears satisfactory.

A quantitative estimate of the differences in wind speeds between U_{VV} and U_{HH} as a function of incidence angle is better illustrated by the two plots of Figure 6. In the left plot the data are sorted into one ms^{-1} U_{VV} wind-speed bins on the abscissa, and then averaged over the corresponding ordinate values. Shown is the difference between the mean value of U_{HH} and the mean value of U_{VV} for each U_{VV} bin. In the right plot, the data are sorted into one ms^{-1} U_{HH} wind speed bins.
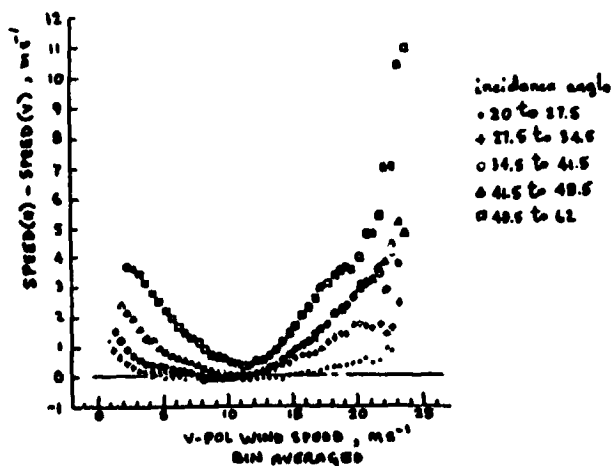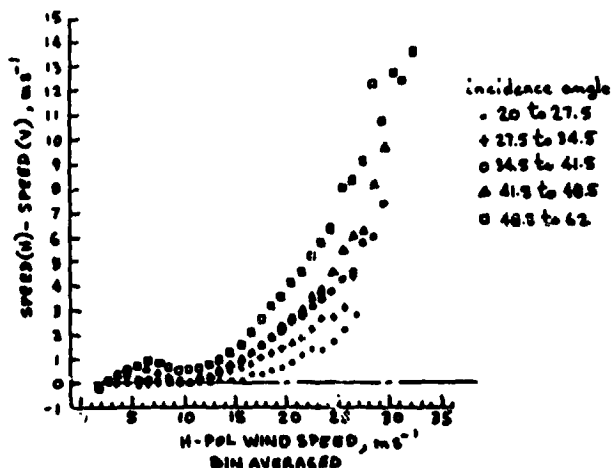

Figure 6. Comparisons of differences between mean values of U_{HH} and U_{VV} as a function of either U_{VV} sorted data (left plot) or U_{HH} sorted data (right plot) for the five different incidence angle bands noted by the symbols at the right of each plot.

64
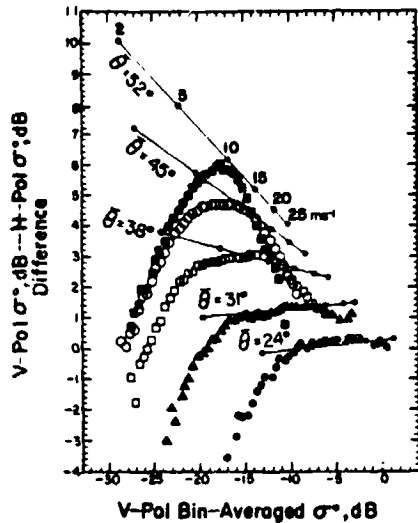
Figure 7. Comparison of differences between mean values of σ_{VV}^{o} and σ_{HH}^{o} as a function of bin averaged σ_{VV}^{o}, all rederived from SASS1 and all the 377,289 pairs of the U_{VV} and U_{HH} data, for the five incidence angle bands centered at Θ values shown. The lines represent the corresponding SASS1 model differences in σ_{VV}^{o} and σ_{HH}^{o} as a function of σ_{VV}^{o} for the five incidence angles. The wind speeds determined from the V-Pol SASS1 model are noted on the top line for a reference.
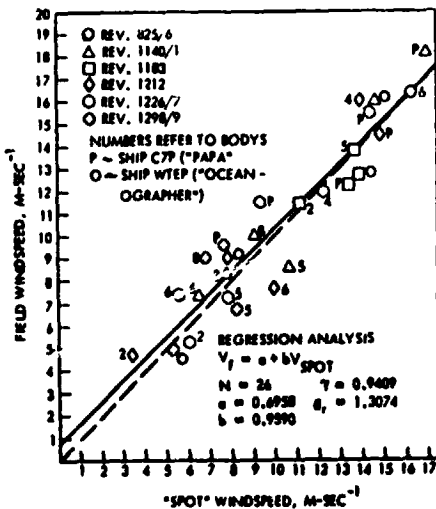

Figure 8. Calibration of the GOASEX-region windfield speeds derived from surface pressure fields to collocated high-quality observations of wind speed from buoys (numbers), research vessels at PAPA (P), and the research ship Oceanographer (O).

The data points are further sorted into incidence angle bands as noted on the plots by coded symbols. Here, all five incidence angle bands are displayed. The best agreements between U_{VV} and U_{HH} for all incidence angles for both binning methods occurs near 10 ms^{-1}, the mid-range of the JASIN wind speed data used to "tune" the SASS1 model function. This data illustrates the lack of consistency between U_{VV} and U_{HH} and shows V-H differences greater than specifications allowed in the error of either polarization type, particularly at the higher winds and larger incidence angles. The differences in both plots for wind speeds less than 10 ms^{-1}, can be partially reconciled by examining the three-dimensional distributions of the U_{HH} and U_{VV} data in Figure 5. The left plot of Figure 6 appears to be more indicative of the trend in the U_{VV}/U_{HH} bivariate distribution mean (approximately given by the ridge top) than is the right plot at lower wind speeds.

Now, is it possible that a minor correction can bring SASS1 into internal conformity? To test this hypothesis, we present the statistical data in a different format. Consider the difference $\sigma_{VV}^{o} - \sigma_{HH}^{o}$. According to the power law formulation, this difference must have the form:

$$\alpha + \beta \log_{10} U \qquad (3)$$

This logarithmic form is seen in the straight lines on Figure 7 plotted according to SASS1 for five incidence angles. The data points corresponding to these incidence angle categories are also plotted as recomputed (i.e. mapped back to units using SASS1 at mid-band incidence angles and the arbitrarily chosen value $\chi = 0$ (upwind) for the azimuth) $\sigma_{VV}^{o} - \sigma_{HH}^{o}$ versus the bin-averaged V-Pole σ_{VV}^{o}. The conclusions of the previous paragraphs are confirmed: the consistency of SASS1 is

65

validated only for a small mid-range of
speeds for the larger incidence angles,
and for a somewhat larger range of
speeds for the smaller incidence
angles. Altogether, the shapes of the
data-curves in Figure 7 strongly
suggest that the power law relationship
of Equation (1) is not an adequate
representation.

4.   COMPARISONS OF SASS1 AND OTHER MODEL PREDICTED WINDS WITH IN SITU
WINDS

     This section will use in situ data to reinforce the conclusions
of the previous section: the power law relationship (1) between NRCS
and wind speed requires revision.

     The primary in situ winds used in this study came from wind
fields analyzed for the GOASEX workshops (Barrick et al, 1980, and
Brown et al, 1982). Figure 8 illustrates the relatively good quality
of the winds from the wind fields when calibrated to buoys in the Gulf
of Alaska (the numbers refer to the last digit of the buoy
identification number; e.g. "2" refers to buoy 46002) and the research
vessels: Oceanographer ("O") and either the Quadra or Vancouver which
were located at ocean station "Papa" ("P") at that time. The symbols
indicate the SASS Rev numbers at the time of the Seasat overflights of
the in situ buoy and ship measurements used in these comparisons. The
abscissa, noted in the figure as the "spot" wind field, represents the
values of these in situ measurements, while the ordinate represents
those from the GOASEX wind fields.

     Plotted in Figure 9a (upper left plot) are the wind speed
comparisons of the winds from SASS (the ordinate) estimated by the
Wentz2 model function (one of the ancestors of SASS1, Barrick et al.,
1980), versus the winds from the GOASEX wind fields (the abscissa).
Each data point represents a bin of 100 independent pairs of
measurements which were sorted along the abscissa, and which were co-
located in space and time within 3 hours of the Seasat overpass. The
bars represent one sample standard deviation for both parameters in
each 100 sample-size bin. Barrick et al. (1980) noted that the G-H
table for Wentz2 was based solely on aircraft-scatterometer/wind-
"truth" measurements. Thus the computed SASS winds in this plot,
derived from a power-law model, were independent of the influence of
any SASS/wind-"truth" calibrations. Note that estimations of the
SASS/Wentz2 wind speeds are generally higher than those from the
GOASEX wind fields. Agreement between these two independent wind
data sets occurs near 18 ms^{-1} where the diagonal (which would
represent perfect agreement) appears to intercept the data.

     The data points in Figure 9b (upper right plot) represent the
same data set as in the upper left plot, except the ordinate values
have been transformed back to NRCS V-Pol values with Wentz2 using

66

Θ = 38 and X = 0. For the latter specification, the Wentz table value for G is - 3.524, and for H is 2.074 (F. J. Wentz, personal communication). For comparison, the SASS1 V-Pol model is plotted (the dashed line through the data points), also for Θ = 38 and X = 0.
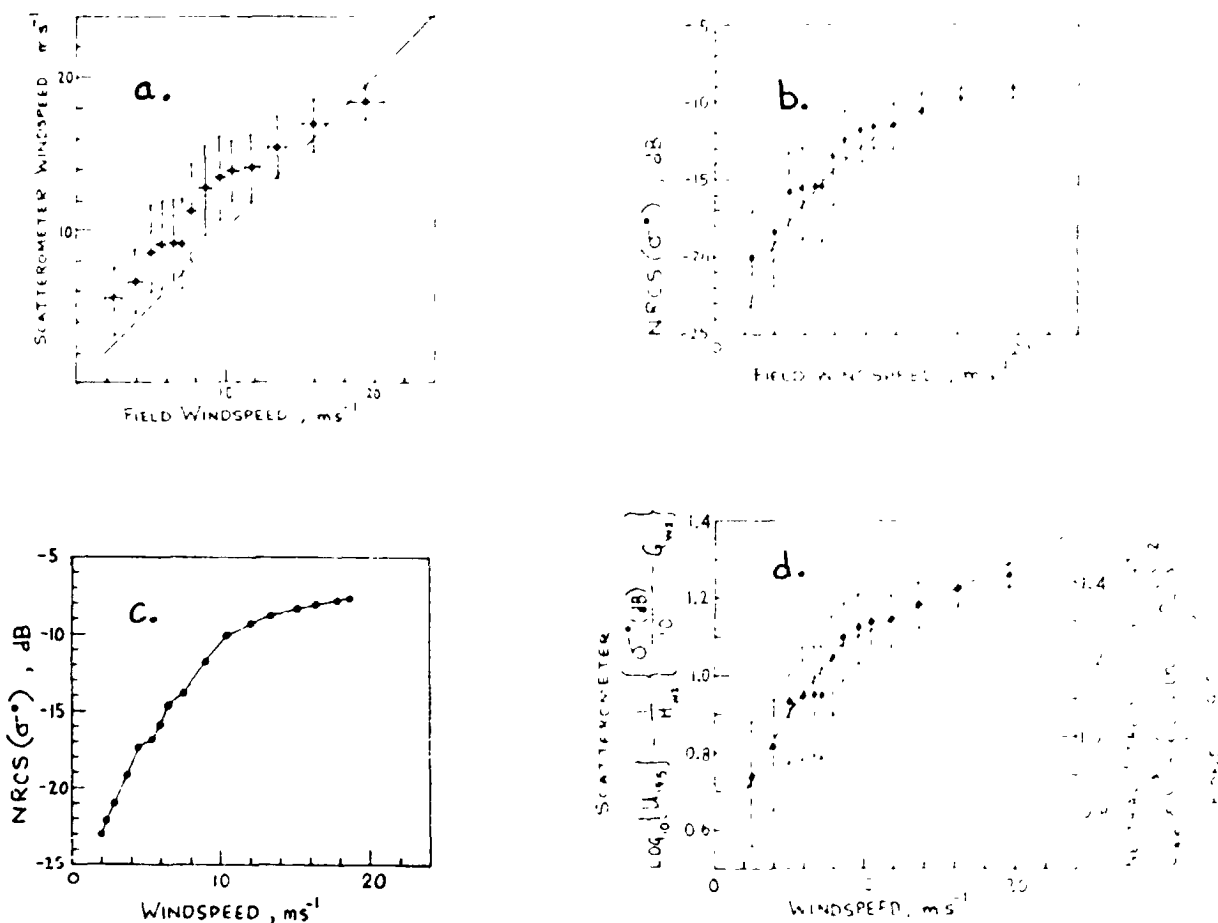
Figure 9. Four plots that essentially compare V-Pol scatterometer-related data (left ordinate), and collocated in situ "truth" data (abscissa): a) The upper left plot compares the results from the GOASEX region to Wentz2 (an ancestor of SASS1) model-derived results. Perfect agreement would be along the diagonal. b) The upper right plot compares results (data points) from the GOASEX region to the SASS1 (dashed line through the data points). c) The lower left plot shows replotted data from Duncan et al. (1974). d) The lower right plot shows comparisons between SASS data (left ordinate vs. abscissa) and Kondo's (1975) empirical model which relates the measurements of the rms heights of the high frequency ocean waves (wavelengths from about 0.8 cm to 62 cm) via the aerodynamic roughness length, l_0, further related to the bulk momentum transfer coefficient, $10^3 C_{19.5}$ (right ordinate), to measured windspeeds.

As previously noted, SASS1 was calibrated to the JASIN wind field data set. The abscissa in Figure 9b thus represents wind values from GOASEX (data points) as well as wind values from JASIN (the SASS1 curve). The horizontal error bars for the GOASEX winds have been left off for clarity. These errors are shown in the upper left plot. However, because of the new scale for the ordinate, the vertical error bars from Figure 9a have been transformed. A comparison of Figures 9a and 9b shows that there is considerable improvement in model fit to the data by the JASIN-calibrated SASS1 over its ancestor.

Wentz2. Although much of the model bias has been removed for the lower wind speeds, SASS1 would appear to underestimate the higher winds. The data of Figure 1, as well as some other case studies (e.g. Jones et al, 1982, Figure 14), appear to confirm the poorer estimates of U_{VV} at higher speeds when a power-law function empirical model is calibrated to fit only the lower wind speed regime (i.e., wind speeds < 16 ms^{-1}).

We now examine the tendencies of the data obtained during the GOASEX period which are displayed in Figure 9b. The mean values of the distributions appear to be rather smoothly varying over the entire range of values with the possible exception of the mean wind speeds located near 7 ms^{-1} . It seems that an empirical model function determined with two, or possibly three, disjoint linear regressions yielding a broken line through the mean wind speeds of the distributions would give better estimates of U_{VV} for both the lower and higher wind speed regimes. It could also be argued that one of the breakpoints connecting the linear fits would occur near 10 ms^{-1} , and perhaps a second near 5 ms^{-1} . Such a model would obviously deviate from a power-law function attempting to cover the entire wind speed regime. In addition , the trend of the mean values suggests that this hypothesized empirical model would result in a σ° vs. wind-speed slope less than predicted by SASS1 for wind speeds greater than 10 ms^{-1} .

The two- or three-regime type scatterometer model function speculated on here could also be suggested for the data shown in Figure 9c (the lower left plot). However, the data shown by the points in this plot resulted from a wind-wave tank experiment reported by Duncan et al. (1974), which included measurements by an X-band (frequency of 9.375 GHz, wavelength of 3.2 cm) scatterometer in the vertical polarization mode. The data in Duncan et al. (their Figure 13) was replotted here with a logarithmic scale in dB for σ°. The authors noted that a "second break point is easily discernible in the data at a wind speed of about 10 m sec^{-1} ", apparently confirming our view that the form of the model function for the vertically polarized SASS data should be other than a single power function over the entire wind speed regime.

The evidence presented thus far at least suggests that the form of the model function relating σ°_{VV} and U_{VV} might be more convex in shape than SASS1, and thus departs somewhat from SASS1 and its ancestors. As seen in Figure 9b, however, SASS1 gives a fair empirical representation of the rate of change of σ° to U over the wind speed range available for its calibration. The perceived inadequacies of SASS1 are probably not due to a lack of quality of the calibration in situ JASIN data used (inasmuch as the JASIN data was the best possibly available), but are perhaps due to the limited quantity and range of environmental conditions available for its calibration. Other shortcomings are noted in Schroeder et al. (1982b., p 3335). A new model, which would correct some of the difficulties with SASS1, is proposed in the following section.

08

5. AN EMPIRICAL MODEL RELATING SCATTEROMETER NRCS TO BOTH WIND AND WIND STRESS

The four plots of Figure 9 form a group of related data. A discuss'on of Figure 9d will involve the proffering of a new empirical scatterometer-model-function parameterization --- the topic cf this section. The new aspects of this parameterization are: (a) the departure from an empirical model based on a power-law function, and (b) the estimation of both wind and wind stress from the NRCS. Previous models only resulted in either an estimation of wind, or an estimatcn of wind stress (Jones and Schroeder, 1978).

The theoretical basis for the parameterization of air-sea interaction is a complex and controversial subject that cannot be entered into here. In cur view, however, the best treatment of the theory and the most appropriate ocean measurements are those of Kondo (1975) and Kondo et al. (1973). His analysis relates the bulk momentum transfer coefficien: C_{10} (since his observations were taken at 10 meters) to the aerodynamic roughness length of the sea surface Z_0, which he describes as related to the rms height of the "sea surface irregulrrities associated with the high frequency ocean waves" with wavelengths from about 0.8 cm to 62 cm. This relationship, of course, derives from the logarithmic wind profile in the surface layer, an assumption commonly accepted over the ocean surface. From his experiments, Kondo then determines C_{10} from the roughness length and relates the drag to the wind speed according to an approximate linear formula. Since our wind data are referred to at a 19.5 meter elevation, we convert Kondo's results to:

$$10^3 C_{19.5} = A + BU = C_*$$ (4)

Kondo (1975) present: : : :nstants for four wind-speed regimes, and also gives formulas :r. :onverting to arbitrary C_z. Thus, the following set of constants are calculated entirely from his work, with no assumptions of our own:

U, ms^{-1} (at 19.5 m)	A	B
2.3 - 5.3	0.71	0.069
5.3 - 8.5	0.80	0.052
8.5 - 26.8	1.08	0.019

We now, however, allow ourselves one adjustable additive constant, S_p, which will then be a function of incidence angle, azimuth angle, and polarization. Then the model function (2) takes the new form:

$$\sigma^\circ(dB) = 10\left\{ G(\theta,\chi,\epsilon) + H(\theta,\chi,\epsilon)\left[C_* - S_p(\theta,\chi,\epsilon)\right] \right\}$$ (5)

69

The adjustable constant S_p was chosen to produce a best fit to the SASS data points of Figure 9d. The results appear in Figure 9d, where the solid line - composed of three segments - is calculated from equation (5) with $S_p = 0.157$.

There are two features to note about Figure 9d. First, owing to the different structures of the three wind-speed regimes, as observed by Kondo (and others), the low and high wind-speed regimes are fit by (5) better than by SASS1, as seen in Figure 9b. Second, because the formulation of Kondo has a physical basis in the similarity theory of the surface layer, it results in the determination of the stress on the sea surface

$$\tau = \rho C_z U_z^2 \tag{6}$$

consistent with, and at the same time as, the wind speed U_z. The appropriateness of this formulation was long ago recognized by Munk (1955), who emphasized that the form drag is essentially determined by the high frequency portion of the ocean wave spectrum owing to the contribution thereof to the mean-squared surface slope.

6. DISCUSSION AND CONCLUSIONS

The stroke of perspicacity resulting in the design of dual-polarization modes for each SASS antenna permitted the possibility of an internal calibration of the SASS1 model function, as demonstrated above. Our study of comparisons between collocated U_{VV} and U_{HH} strongly suggests that the power-law relationship of equation (1) is not an adequate representation. But, if the proper function for determining U_{VV} or U_{HH} becomes known, the other could be defined. The results at the higher wind range were anticipated by Valenzuela (1968). Wright (1966, and 1968), from his comparative studies of σ_{VV}^o and σ_{HH}^o, suggested that the major behavioral differences between σ_{VV}^o and σ_{HH}^o as a function of incidence angle and wind speed could be explained by the much stronger dependence of σ_{HH}^o than σ_{VV}^o on sea slope. In addition, Wright showed that this characteristic difference leads to an estimate of the mean-squared slope of the sea surface.

The data analysis performed in Section 3, i.e., the comparisons between SASS1 and other model-predicted winds with _in situ_ winds, reinforce the results of Section 2. Further, the evidence provided by the data at least shows that the model relating σ_{VV}^o to U_{VV} is more convex in form than the SASS1 form, a result which could be anticipated by the experimental data of Duncan et al (1974). This observation about the σ_{VV}^o vs U_{VV} form, plus that about the relative change of σ_{VV}^o with σ_{HH}^o, Figure 7, leads to the conclusion that H-Pol backscatter shows greater sensitivity to wind speed variation at higher winds, and less at lower winds, than does V-Pol backscatter.

The data analysis in Section 2 and 3 above clearly suggests that further SASS1 model function adjustments are still required if the Seasat scatterometer wind specifications are to be met over the entire range of wind speeds (4 to 24 ms^{-1}), particularly for winds greater than 16 ms^{-1}. The GOASEX winds, although of less quality than those from JASIN, proved to be beneficial in this evaluation and in the formulation of the proposed new model (Section 4) because of the larger dynamic range of environmental conditions available, and because of the larger statistical sample. Our new model fits the data better than SASS1, particularly for the higher wind speed range.

The understanding of the physics of the NRCS and its interaction with the ocean surface is an air-sea interaction problem - a complex and controversial subject. In addition, meteorologists are largely interested in the marine winds, while oceanographers are largely interested in the wind stress. Previous SASS models only led to the computatic of one of these geophysical parameters. For SASS1, the output was the marine wind speed. Herein, both the meteorologists and oceanographers are presented a consistent formulation, Equations (4), (5), and (6), of a model function that results in the estimation of both the wind speed and wind stress from SASS measurements.

The new empirical model has a more physical basis for its development and formulation that its predecessor, SASS1. In our formulation, the NRCS is related to the aerodynamic roughness length through the bulk momentum transfer coefficient (right scale of Figure 9d). The aerodynamic roughness lengths, as noted by Kondo (1975), are based on measurements of the rms height of the amplitude of ocean waves between about 0.8 to 62 cm in wavelength. These were then correlated to measured winds by Kondo through the bulk momentum transfer coefficient. Scattering theory shows that the NRCS is a measure of the mean-squared amplitude of the Bragg resonant scattered ocean waves (Wright and Keller, 1971). For SASS, these Bragg resonant waves are between about 1 to 3 cm in wavelength (for incidence angles 60 to 20 degrees, respectively). It therefore may not be surprising that the rate of change of the NRCS with wind speed and the rate of change of the bulk momentum transfer coefficient of Kondo (1975) with wind speed is strongly correlated (correlation coefficient of 0.99). Whether Kondo's empirical parameterization adequately represents the wind stress is a matter for future verification. Even so, Garratt (1977) noted that the bulk momentum transer coefficient of Kondo "based on high-frequency wave amplitude data, agrees well with the collected C_{DN} data".

The ocean wavelength regimes discussed above neatly straddle the capillary-gravity wavelength range. In the theories of capillary-gravity wave propagation, viscosity and surface tension play an important role and should be taken into consideration for future scatterometers as well as for SASS. Over a global ocean surface temperature range of 25C the viscosity of sea water varies by a factor of two: this variation affects the short wave structure and thence possibly the backscatter which is sensitive o these waves. Our continuing work on the parameterization of the model function includes the incorporation of both viscosity and surface tension.

71

Spaceborne scatterometer systems are now being considered necessary by NASA and the Navy for future satellites. ESA (European Space Agency) has already approved a spaceborne mission which includes a scatterometer. Our research, which includes studies to characterize the errors as well as the important scatterometer-related physics, are potentially important to the design, implementation, and utilization of future spaceborne scatterometers, and to an understanding of the role of scatterometry in global meteorological and oceanographic research, applications, and predictions.

7. ACKNOWLEDGEMENTS

8. REFERENCES

Barrick, D. E., P. M. Woiceshyn, J. C. Wilkerson, G. H. Born and D. B. Lame, 1980: SEASAT Gulf of Alaska workshop II report. JPL Int. Doc. 622-107, Jet Propulsion Laboratory, Pasadena, CA.

Boggs, D. H., 1981: The Seasat scatterometer model function: the genesis of SASS1. JPL Int. Doc. 622-230, Jet Propulsion Laboratory, Pasadena, CA.

Boggs, D. H., 1982: Geophysical data record (GDR) users handbook. JPL Int. Doc. 622-232, Jet Propulsion Laboratory, Pasadena, CA.

Brown, R. A., 1983: On a satellite scatterometer as an anemometer. J. Geophy. Res., 88, 1663-1673.

Duncan, J. R., W. C. Keller, and J. W. Wright, 1974: Fetch and wind
    speed dependence of Doppler Spectra. Radio Science, 9, 809-819.

Fett, R. W. and W. A. Bohan, 1981: Navy tactical applications guide,
    vol. 3. NEPRF Tech. Report 80-07, Naval Environmental Prediction
    Research Facility, Monterey, CA

Garratt, J. R., 1977: Review of drag coefficients over oceans and
    continents. Mon. Wed. Rev., 105, 915-929.

Hibbs, A. R., and W. S. Wilson, 1983: Satellite map of the oceans.
    IEEE Spectrum, 20, No. 11, 46-53.

Jones W. L. and L. C. Schroeder, 1978: Radar backscatter from the
    ocean: dependence on surface friction velocity. Bound.-Layer
    Meteor., 13, 133-149.

Jones, W. L. and L. C. Schroeder, D. H. Boggs, E. M. Bracalente, R. A.
    Brown, G. J. Dome, W J. Pierson and F. J. Wentz 1982: The SEASAT-
    A satellite scatterometer: the geophysical evaluation of remotely
    sensed wind vectors over the ocean. J. Geophys. Res., 87, 3297-
    3317.

Kondo, J., Y. Fujinawa and G. Naito, 1983: High-frequency components
    of ocean waves and their relation to the aerodynamic roughness.
    J. Phys. Ocean., 3, 197-202.

Kondo, J., 1975: Air-sea bulk transfer coefficients in diabatic
    conditions. Bound.-Layer Meteor., 9, 91-112.

Moore, R. K. and A. K. Fung, 1979: Radar determination of winds at
    sea. Proc. of IEEE,. 67, 1504-1521.

Schroeder, L. C., W. L. Grantham, J. L. Mitchell and J. L. Sweet,
    1982a: SASS measurements of the Ku-band radar signature of the
    ocean. IEEE J. Oceanic Eng., OE-7, 3-14.

Schroeder, L. C., D. H. Boggs, G. J. Dome, I. M. Halberstam, W. L.
    Jones, W. J. Pierson and F. J. Wentz, 1982b: The relationship
    between wind vector and normalized radar cross section used to
    derive SEASAT-A satellite scatterometer winds. J. Geophys. Res.,
    87, 3318-3336.

Peteherych, S., M. G. Wurtele, P. M. Woiceshyn, D. H. Boggs and R.
    Atlas, 1984: First global analysis of SEASAT scatterometer winds
    and potential for meteorological research. These proceedings.

Valenzuela, G. R., 1968: Scattering of electromegnetic waves from a
    tilted slightly rough surface. Radio Science, 3, 1057-1066.

Valenzuela, G. R., M. B. Laing, and J. C. Daley, 1971: Ocean spectra
    for the high-frequency waves as determined from airborne radar
    measurements. J. Marine Res., 29, 69-84.

Wright, J. W., 1966: Backscattering from capillary waves with

application to sea clutter.   IEEE Trans. on Ant. and Prop., AP-14, 749-754.

Wright, J. W., 1968:   A new model for sea clutter. IEEE Trans. on Ant. and Prop., AP-16, 217-223.

Wurtele, M. G., P. M. Woiceshyn, S. Peteherych, M. Borowki and W. S. Appleby, 1982:   Wind direction alias removal studies of SEASAT scatterometer-derived wind fields.   J. Geophys. Res., 87, 3365-3377.

Wright, J. W. and W. C. Keller, 1971: Doppler spectra in microwave scattering from wind waves. The Physics of Fluids, 14, 466-474.